Journal of
Materials Chemistry A

ROYAL SOCIETY OF CHEMISTRY

Hierarchical Nickel/Phosphorus/Nitrogen/Carbon Composites Templated by One Metal–Organic Framework as Highly-Efficient Supercapacitor Electrode Materials

Journal:	*Journal of Materials Chemistry A*
Manuscript ID	TA-ART-12-2018-011568.R1
Article Type:	Paper
Date Submitted by the Author:	23-Dec-2018
Complete List of Authors:	Yu, Fan; Jianghan University, School of chemistry and environmental engineering xiong, xin; Jianghan University, School of chemistry and environmental engineering zhou, liuyin; Jianghan University, School of chemistry and environmental engineering Li, Jialuo; Texas A&M University, Chemistry Liang, Ji-Yuan; Jianghan University, School of chemistry and environmental engineering Hu, Si-Qian; Jianghan University, School of Chemistry and Environmental Engineering, Key Laboratory of Optoelectronic Chemical Materials and Devices of Ministry of Education Lu, Wangting; Jianghan University Li, Bao; Huazhong Univ Sci , ; huazhong university of science and technology Zhou, Hong-Cai; Texas A&M University, Chemistry

SCHOLARONE™
Manuscripts

Journal Name

ARTICLE

Hierarchical Nickel/Phosphorus/Nitrogen/Carbon Composites Templated by One Metal-Organic Framework as Highly-Efficient Supercapacitor Electrode Materials

Fan Yu[a],*, Xin Xiong[a], Liu-Yin Zhou[a],Jia-Luo Li[c], Ji-Yuan Liang[a], Si-Qlan Hu[a], Wang-Ting Lu[a], Bao Li [b,c],* and Hong-Cai Zhou*[c]

Abstract: By utilizing the proper template of Metal-Organic Frameworks (MOFs) for fabricating high performance supercapacitor electrodes have been emerging a great attention. But rare attention has been paid onto how to prepare the excellent MOF template for deriving the anticipated electrode materials. Herein, one two-fold interpenetrating MOF, had been successfully constructed, along with microporous structure and multi-components as nickel, phosphorus, nitrogen, oxygen and carbon in the final framework. The pristine sample could be directly utilized as supercapacitor electrode materials, which exhibits the moderate electrochemical capacitance of 979.8 F g^{-1} at a current density of 1 A g^{-1}. By the simple treatment of one-step pyrolysis in the nitrogen atmosphere at different annealing temperature (500°C, 600°C, 700°C, 800°C), rare hierarchical Ni/P/N/C composites, denoted as Ni/P/N/C-500, Ni/P/N/C-600, Ni/P/N/C-700, Ni/P/N/C-800, have been derived from the parent MOF. The anticipated multi-components of Ni, P, N and O have been uniformly incorporated into carbon materials, which would result in excellent synergistic effect to improve the performance of electrochemical energy storage. The morphologies and components of these derivatives have been characterized via SEM, XPS and XRD, indicating the uniform distribution of different components in the hybrid structures. The maximum specific capacitance of Ni/P/N/C-500 electrode could reach 2887.87 F g^{-1} at a current density of 1 A g^{-1}, superior to the other hierarchical composites and setting up a new benchmark in the related field. The combination of several advantages in these derivatives, such as a high surface area, even distribution and ultrahigh content of Ni/P/N/C components, ensure their high-performances in energy storage. The presented results fully demonstrate the unique advantage of utilizing the pre-designed MOFs as a template to prepare the hybrid materials used as the potential electrode-active materials in supercapacitors, and provide an efficient route to fabricate the superior performance energy storage devices.

Introduction

The energy and environmental crisis has seriously affected the current economic and social development. As a new type of clean energy, how to efficiently store and utilize electrical energy becomes the core technique to solve the ineluctable energy crisis in the next years.[1-4] Normally, the current forms

[a.] *Key Laboratory of Optoelectronic Chemical Materials and Devices of Ministry of Education, School of Chemical and Environmental Engineering Jianghan University, Wuhan, 430056，PR China. *Email:yufan0714@163.com.*

[b.] *Key laboratory of Material Chemistry for Energy Conversion and Storage, School of Chemistry and Chemical Engineering, Huazhong University of Science and Technology, Wuhan, Hubei, 430074, PR China. *E-mail: libao@hust.edu.cn.*

[c.] *Department of Chemistry, Texas A&M University, College Station, Texas 77843-3255, United States. *E-mail: zhou@chem.tamu.edu.*

of utilizing the electrical energy contain solar cells, fuel cells and batteries, which have been commercialized and widely used.[5-6] The traditional batteries would not only supply a high density of electrical energy, but also provide the longer energy life. However, the power density of traditional batteries is normally poor, which may be ascribed to the nature of slow redox process and sluggish rate of ion migration via the electrode-active materials.[7-9] Compared to the traditional batteries, supercapacitor, as a booming class of electrochemical energy storage devices, have received more and more attention, since supercapacitors usually have higher power density and longer cycle life.[9-13] The energy storage mechanism of supercapacitors is generally deemed as that electrons could be stored onto the surface of electrode-active materials through the adsorption of electrolyte ions.[14-17] Nowadays, most of the electrode-active materials concentrate on the carbon materials, which normally exhibit the low capacitance due to the low specific surface area (SSA), single adsorption active-sites and bad conductivity.[18-21] Through the presented results, it has been revealed that the introduction of hetero-components, such as metal/metal oxide, nitrogen,

phosphorus or oxygen, into carbon materials would effectively enhance the capacitance.[22-26] The combination of hetero-components into carbon materials would motivate the pseudocapacitive effects, promote the wettability to electrolyte solution and enhance the conductivity.[27-30] Therefore, the effective fabrication of uniform multi-components carbon materials has become the main target for the development of supercapacitor electrode-active materials.

Metal-Organic Frameworks (MOFs), as a very attractive organic-inorganic hybrid material, has the characteristics of structural- and surface-tunability, and has shown excellent application prospects in many fields.[31-33] Recently, pristine MOFs or MOF-based carbon derivatives have been explored to utilize as the electrode-active materials of supercapacitors due to the specific characteristics of MOFs materials, such as versatile selection of organic linkers and metal nodes, inherent porosities, uniform distribution of multi-components and facile treatments of the related materials.[34-36] Through the reported results, it has been validated that MOFs could be of the ideal pyrolysis templates to prepare the anticipated electrode-active materials. Compared to the traditional porous carbon-based electrode-active material, the MOFs-based derivatives exhibit the very unique traits: To improve the performance, the pre-designed multi-components could be easily introduced into the final hybrid materials; the types and proportions of the doped hetero-components could be modulated via the very facile handling; more importantly, the doped elements could be evenly distributed due to the effective spacing and regular arrangement.[37-40] All of these traits endow MOF-based derivatives excellent electrochemical activity, which have been widely used as the high-performance electro-active materials.[10-18]

However, most of the reported results had been concentrated on the utilization of the several star MOFs, and only one or two types of hetero-components could be effectively introduced into the final carbon materials, such as N, O or metal/metal oxides.[41-43] In the reported derivatives fabricated from the pristine MOF, rare samples, which simultaneously emerge elements of metal, P, N and O into one carbon materials, had been reported due to the limited selection of pristine MOF materials. The element of P is usually introduced via the post-modification method. Thus deficiency means that the excellent advantages of MOFs, such as the structural diversity and adjustability, had been not yet adequately utilized in the field of electrochemical energy storage. In order to reflect the richness of structural characteristic and tunable components of MOFs, more and more innovative works, including the effective construction of new pristine MOFs, the variable conditions of preparing MOF-based derivatives and the rational design of sacrificial templates, are urgently requested to be presented.[44-47] It is well known that if the pre-selected organic linkers for assembling MOFs could contain the anticipated components, multi-component hybrid electrode materials could be effectively fabricated via the specific processing methods. In addition, it has been proven that the nickel-based derivatives derived from Ni-MOFs could exhibit the high performance of

super-capacitance effect due to the induction of pseudocapacitive effects and high rate capability.[46-47] Therefore, with the comprehensive consideration of the advantages of the multiple components, the types of composite derivatives, exampled as Nickel/Phosphorus/Nitrogen/Carbon composites, might exhibit the higher level of synergistic effect to improve the performance of the supercapacitance.
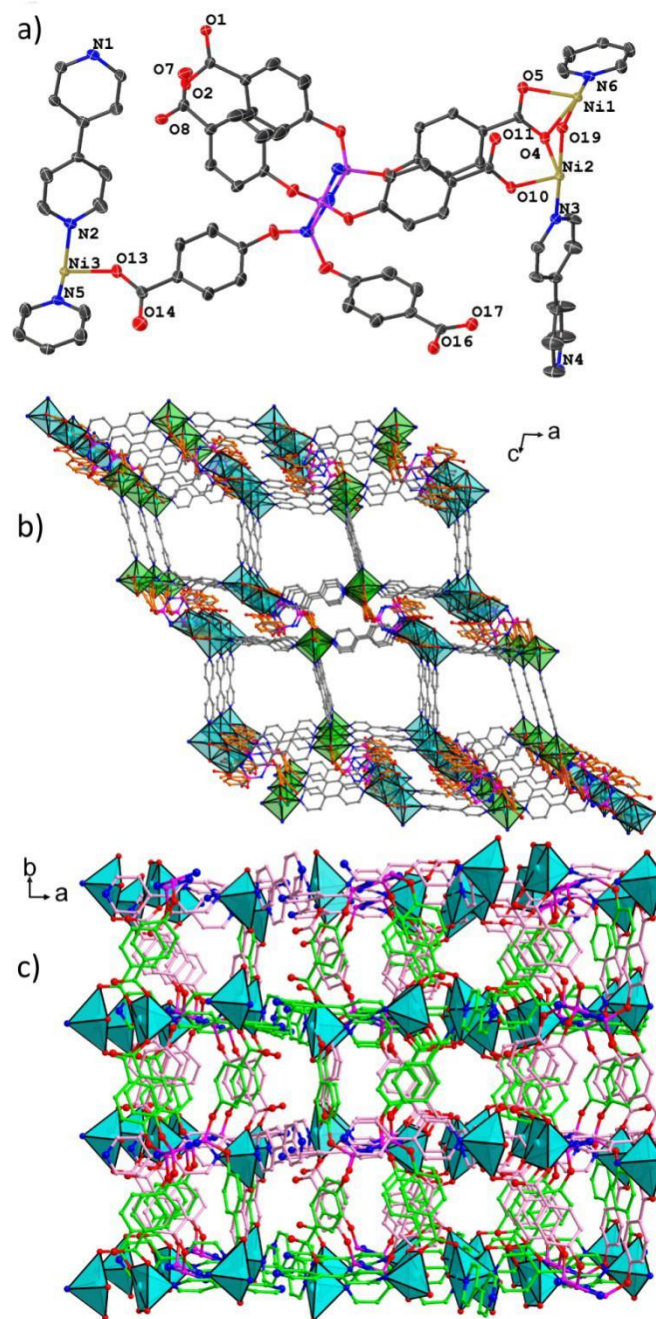
Figure 1. (a) Perspective view of asymmetric unit of Ni-MOF; (b) Partial view of the single framework of Ni-MOF along *b*-axial direction; (c) Partial view of the two-fold interpenetrating structure of Ni-MOF along *c*-axial direction.

To verify the practicality of the above hypothesis, a hexa-carboxylate ligand, hexakis(4-formylphenoxy)

cyclotriphosphazene (H_6L1), which contains the multiple elements of C, P, N and O, had been selected to react with nickel ions to build the highly-ordered crystalline sample. The resulted MOF material could serve as the parent template to fabricate the hybrid derivatives simultaneously combining Ni, P, N, C and O elements into one material via one-step treatment. Herein, a two-fold interpenetrating MOF, [$Ni_3(H_2O)(bpy)_3(L1)$] (**1**, bpy = 4,4'-bipyridine), had been successfully constructed via solvothermal method. The purpose of introducing bpy is to ensure the formation of Ni-N surrounding and porous structure. Subsequently, the pristine template could be further converted to the anticipated multi-component hybrid materials via the method of pyrolysis at different temperatures (500, 600, 700 and 800 ℃), labelled as Ni/P/N/C-500, Ni/P/N/C-600, Ni/P/N/C-700 and Ni/P/N/C-800. The pristine MOF and hierarchical hybrid composites after annealing at different temperatures have been utilized as electrode-active materials of supercapacitance, which illustrate the high efficient and tunable electrochemical performances related with the characteristics of derivatives. The synthesis, crystal structure, characterization of morphologies and components and the performance of electrochemical storage of each sample had been detailed.

Results and discussion

Description of the crystal structure of pristine MOF 1

The pristine crystal sample of Ni-MOF **1** had been constructed via solvothermal method. The rod-like green crystal samples could be directly obtained via the solvothermal method at 120 ℃ for 2 days. The strong peaks around the positions of 1615 and 1385 cm^{-1} in the IR spectrum clearly illustrate the full deprotonation of carboxyl groups, in consistent with the presented results of crystallographic studies. Through the scanning electron microscopy (SEM) image (Figure 2), the uniform distribution of nickel, phosphorus, nitrogen, carbon and oxygen elements could be detected due to the long-range order nature of MOF material, which is very essential for the synthesis of the subsequent hybrid derivatives.

The X-ray crystal data of Ni-MOF **1** had been collected at room temperature, and the detailed parameter had been listed in Table S1. **1** crystallizes in monoclinic space group $P2_1/c$, whilst the asymmetric unit consist three nickel ions, one complete hexa-carboxylate linkers, three bpy ligands and one coordinated water molecule (Figure 1a). Each nickel ion is hexa-coordinate and adapts the distorted octahedral configuration, which is surrounded by different coordinated atoms. For Ni(1) ion, the coordination sites are occupied by two N-atoms of *cis*-pyridines and four O-atoms from two carboxylate groups with different modes (one μ_2-η^2:η^1 and one *syn-syn*) and one μ_2-bridge water molecule; For Ni(2) ion, the coordination sites are occupied by one N-atom of pyridine and five O-atoms from four carboxylate groups with different modes (two mono-dentate, one μ_2-η^2:η^1 and one *syn-syn*) and one μ_2-bridge water molecule; For Ni(3) ion, the coordination sites are occupied by three neighboring N-atoms of pyridine

and three O-atoms from two carboxylate groups with different modes (one mono-dentate and one chelating). Ni(1) and Ni(2) atoms are interlinked together via water bridge and two carboxyl groups (*syn-syn* and μ_2-η^2:η^1) to form the di-nuclear node, which is further extended via three bpy and two hexa-carboxylate ligands; whilst Ni(3) atom acts as the single-atom node, which is further extended via three bpy and two hexa-carboxylate ligands. The Ni-O and -N bond lengths fall in the range of 2.059(2) to 2.227(1) Å, similar to the typical values of Ni(II) state.[48-49] In these two nodes, two of the parallel bpy linkers connect one di-nuclear node and single-atom node, and the perpendicular bpy linker bind the same node. In addition, the hexa-carboxylate ligand utilizes its six benzoate arms to bind two di-nuclear and two single atom nodes in one plane with the range of distorted $C_{carboxyl}$-$O_{substituted}$-$P_{central}$ angles from 52.1 to 140.2º. In this way, one three-dimensional framework with 1D dimensional channel had been constructed via the reticular connections between nodes to assemble the 4,5-connected *sqc65* topological network with the point (Schläfli) symbol $\{4^2 \cdot 6^4\}\{4^3 \cdot 6^7\}_2$ calculated with *TOPOS* software.
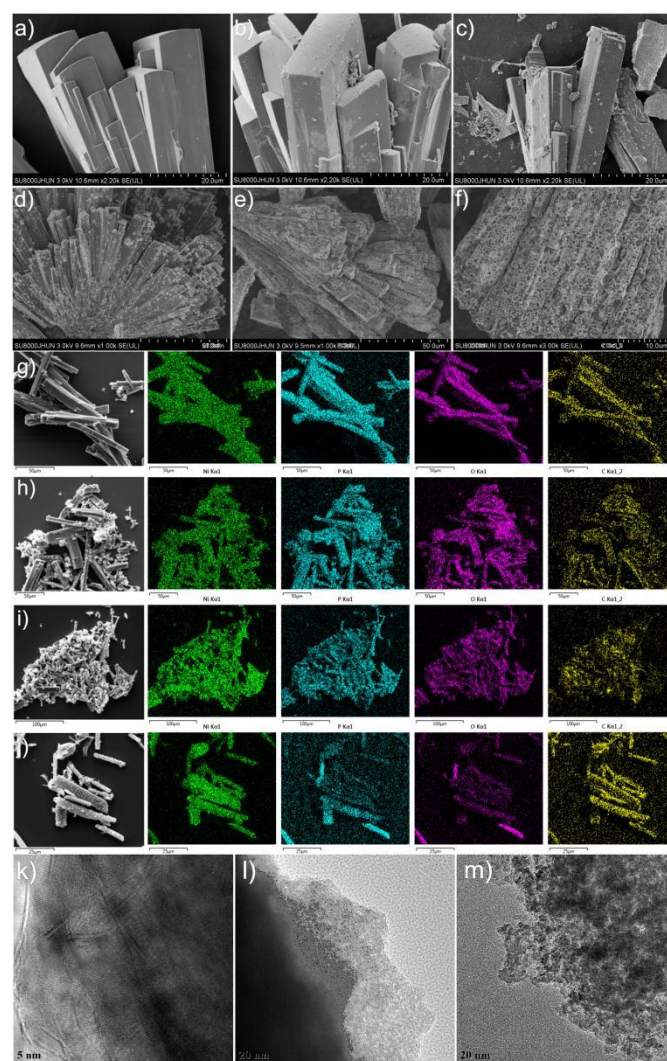
Figure 2. SEM images of pristine MOF (a), hierarchical derivatives, Ni/P/N/C-500 (b), Ni/P/N/C-600 (c), Ni/P/N/C-700 (d) and Ni/P/N/C-800 (e) along with the enlarged

image of Ni/P/N/C-800 (f); (g-j) EDX mapping image of Ni, P, O and C elements in hierarchical derivatives, Ni/P/N/C-500, Ni/P/N/C-600, Ni/P/N/C-700 and Ni/P/N/C-800; (k-m) TEM images of pristine MOF, Ni/P/N/C-500 and Ni/P/N/C-700.

The presence of large channel is further blocked by the same framework to form the dense packing structure. The porosity has been decreased or blocked and ionic diffusion through the MOFs is curtailed, which is estimated as 18.7% according the report of *PLATON* routine. Viewed from the regular crystal structure, the anticipated elements have been captured into the Ni-MOF, which distribute uniformly and have been effectively separated by the organic linkers. These characteristics of the titled MOF satisfy the criteria for preparing the electrode derivatives, and encourage us to investigate the possibilities as the sacrificial template via the method of pyrolysis.
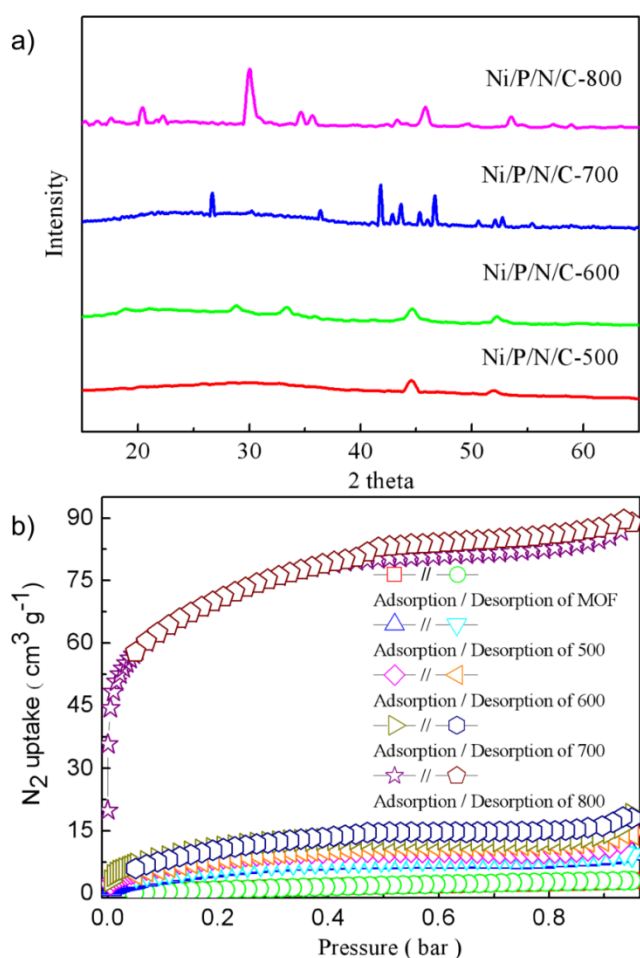
Figure 3. XRD patterns (a) and N_2 sorption isotherms at 77K (b) of hierarchical derivatives, Ni/P/N/C-500, Ni/P/N/C-600, Ni/P/N/C-700 and Ni/P/N/C-800.

The purity of the as-synthesized crystalline sample had been validated by XRD measurement, which shows the matched spectra between the fitted and experimental results. To determine the pyrolysis temperature, the thermal behavior of crystalline sample had been investigated via thermogravimetric analyses (TGA) under N_2 atmosphere (Figure S2). For **1**, the weight loss from 35 °C to 220 °C should

be ascribed to the loss of lattice molecules as water and DMF molecules. The framework could retain up to 400 °C, and then begin to decompose rapidly. The highly connection mode, interpenetrating framework and dense crystal structure must be responsible for the high thermal stability of Ni-MOF. Therefore, the pyrolysis temperatures for the pristine crystalline sample had been determined as 500, 600, 700 and 800 °C according to the thermal stability of the title Ni-MOF.
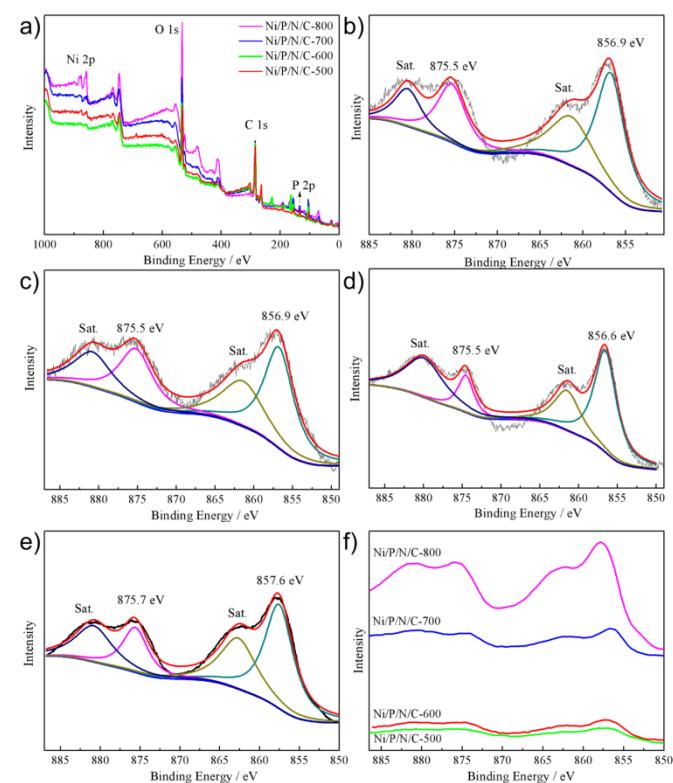
Figure 4. Overall XPS spectra of hierarchical derivatives (a); Ni XPS spectra of Ni/P/N/C-500 (b), Ni/P/N/C-600 (c), Ni/P/N/C-700 (d) and Ni/P/N/C-800 (e) along with the intensity comparison (f).

Synthesis and morphology of hierarchical derivatives

The obtained crystalline samples were directly utilized for the characteristics and as the sacrificial template to derive the other pyrolysis products at different temperatures. Under the nitrogen atmosphere, the pristine MOF material had been annealed at 500, 600, 700 and 800 °C for two hours to fabricate the hierarchical derivatives, which have been utilized for the further characteristics and measurements. The series of hierarchical derivatives could not only still reserve the intrinsic rod-like shape of original sample, but also illustrate the rougher surface along with the obvious porous structure via SEM images (Figure 2). The surface of Ni/P/N/C-500 and -600 is smooth, whilst Ni/P/N/C-700 and -800 is rough, which might be caused by the agglomeration of metal nano-particles to form larger ones along with the increasing carbonization temperature.[50-52] More importantly, the different anticipated elements, Ni, P, N, O and C, could be reserved and distribute uniformly in the fabricated hybrid materials with the tunable ratio from the constructed sacrifice template via element EDS mapping (Figure 2), which would significantly improve the

synergistic effect of the materials and improve the effect in electrochemical performance. To further explore the detailed structures, the pristine MOF, Ni/P/N/C-500 and Ni/P/N/C-700 were also observed via TEM, as shown in Fig. 2k-l and S10. All of these samples exhibit the porous structure. In accordance with the SEM results, the surface of Ni/P/N/C-700 is more rough compared to Ni/P/N/C-500, leading to the larger specific surface area caused by the higher thermolysis temperature.

After the thermal treatment, the original XRD diffraction peaks of Ni-MOF could not be presented (Figure 3). Inversely, for Ni/P/N/C-500, two peaks around 44.5° and 51.8° should be assigned to the (111) and (200) of metallic Ni^0 cubic phase, along with the broad peak of graphite around 26°.[53-55] When the increasing of calcination temperature up to 600 ℃, different types of composite material had been obtained, which exhibits the characteristic peaks as 44.5° (111) and 51.8° (200) of metallic Ni^0 cubic phase, 27.34° (101) and 31.73° (002) of Ni_2O_3 and broad peak of graphite.[55-58] The weak intensity of the two peaks indicate the low content of metallic Ni state in these two different samples. Comparably, for the derivative obtained at 700℃, the strong typical (002) peak of graphite around 26.6° could be detected, along with the other graphite peaks of 36.5° (111), 42.3°(100), 46.3°(012). Whilst partial nickel centers became the state of Ni_3C inferred from two peaks around 41.75°(006) and 44.52°(113).[59-61] The assignment of XRD peaks for sample annealed at 800 ℃ was inexecutable due to the in-matched peak positions compared to the reported Ni species. However, the XRD pattern is very similar to the species of $MnCoNiO_4$ obtained by the thermolysis of $MnCoNiCO_3$ precursor, such as 20.28° (111), 29.96° (220), 34.61° (311), 35.77° (222) and 45.66° (400).[62] Obviously, the different annealing temperatures play the important role in leading to the hierarchical derivatives with different morphologies and compositions.
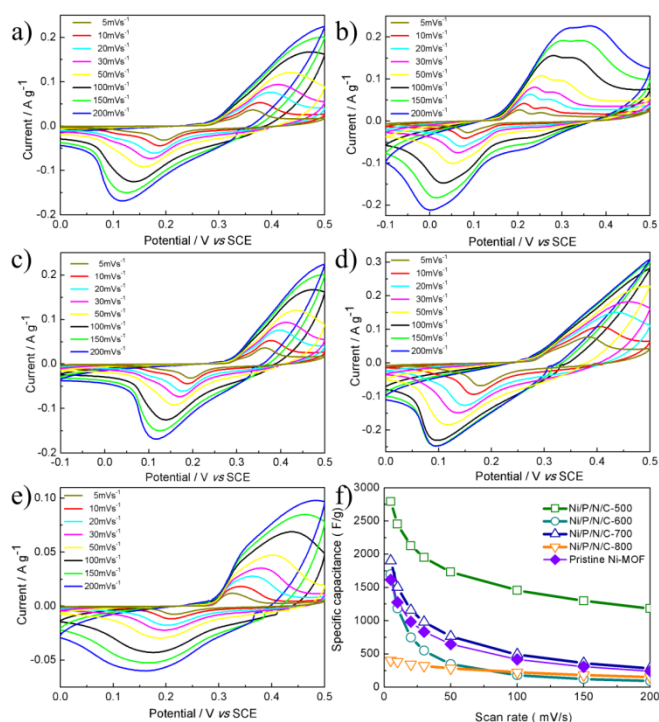
Figure 5. Cyclic voltammogram curves of different electrodes containing pristine MOF (a), Ni/P/N/C-500 (b), Ni/P/N/C-600 (c), Ni/P/N/C-700 (d) and Ni/P/N/C-800 (e) at different scan rates in the range of 5-200 mV s−1; (f) The comparison of specific capacitance of five fabricated electrodes at different scan rates.

The SSA and detailed porous structure of the different hierarchical Nickel/Phosphorus/Nitrogen/Carbon composites had been also investigated via N_2 adsorption-desorption at 77 K (Figure 3). No adsorption behavior for the activated Ni-MOF could be observed due to the collapse of framework in vacuum condition. For Ni/P/N/C-500, 600 and 700, the N_2 adsorption-desorption isotherm shows a typical type-IV curve with the hysteresis effect in the pressure range from 0.5 to 0.95 bar, along with the gradually increasing adsorption amount. Differently, Ni/P/N/C-800 exhibits the type-I adsorption isotherms with a small hystersis, indicating the micro-porous materials, in accordance with the morphology studies in SEM studies. The pore size distribution of different Ni/P/N/C derivatives had been shown in Figure S3, illustrating the micro-porous structure that provide enough surfaces for the process of electron adsorption-desorption in the electrode of supercapacitors.

The series of Ni/P/N/C derivatives had been further analyzed via XPS measurements, as shown in Figure 4 and Table S3. For all of these samples, the signals of Ni, P, N, O and C could be clearly investigated in each spectrum. In each spectra, the major peaks around 857 eV and 875 eV should be ascribed to Ni 2p3/2 and Ni 2p1/2, along with the satellite peaks of Ni 2p3/2 and Ni 2p1/2 around 862 eV and 881 eV, respectively. The low content of metallic nickel state in Ni/P/N/C-500 and Ni/P/N/C-600 might be responsible for the absence of the related peaks.[63-64] Furthermore, the increasing XPS intensity and ICP-OES analysis (Table S4) of nickel

element indicate the increasing content of nickel component in different derivatives.

Electrochemical performance of hierarchical derivatives

The structural characteristics of multi-components and specific porous volumes endow the hierarchical derivatives with the potential possibilities as the electrode-active materials in high-performance supercapacitor. To systematically explore the capacities and set up the relationship between the performances and constitutions, pristine MOFs and hierarchical derivatives had been fabricated as active electrodes which had been investigated by cyclic voltammetry (CV), charge-discharge curves and galvanostatic charge-discharge (GCD) cycling tests with the electrolyte of 6 M KOH and a three-electrode configuration.

Firstly, the CV curves for each sample had been collected with scan rates varied from 5 to 200 mV s^{-1}, which had been shown in Figure 5. At a scan rate of 5 mV s^{-1}, the apparently reversible redox peaks could be detected around 0.35 V and 0.1V, excepted for Ni/P/N/C-500 around 0.25 V and 0.0 V. The different metal state, especially the Ni atom in Ni/P/N/C-500, must be responsible for the different appearance of redox peaks, which indicates the mechanism of pseudo capacitive behavior caused by the redox reactions of the metal ions during the test process.[44-49] Along with the increasing trend of the scan rate up to 200 mVs^{-1}, the separation of the redox peaks are gradually widened because of the small over potential of the electrode. In addition, due to the restriction of mass transfer or ionic transportation at high scan rates, CV curves from 100 to 200 mV s^{-1} get deformed, and the redox peaks disappear gradually, except for the still apparent redox peaks for Ni/P/N/C-500. The reservation of apparent redox peaks clearly illustrates the good rate capability of Ni/P/N/C-500 compared to the pristine MOF and other derivatives. In addition, according to the equation of $C = \int IdV/2\upsilon\Delta Vm$ (the parameters of I, ΔV, υ and m represent the instant current, potential change, scan rate and sample mass, with the unit of A, V, mV s^{-1} and g, respectively), the specific capacitance C (farads per gram) for the prepared electrodes could be conducted from the measured CV curves at different scan rate, as shown in Figure 5f. The calculated specific capacitance of prepared electrodes are 1616.7, 2791.6, 1699.3, 1901.9 and 402 F g^{-1} at the scan rate of 5 mV s^{-1} for pristine MOF, Ni/P/N/C-500, Ni/P/N/C-600, Ni/P/N/C-700 and Ni/P/N/C-800, and then decrease apparently. Observed from the primary results, the electrode containing Ni/P/N/C-500 illustrates the best performance compared to other ones, reflecting the important role of the fabricated components in affecting the corresponding behaviour in electrochemical energy storage.

To further compare the different performance and illustrate the role of component states in electrochemical energy storage, galvanostatic charge-discharge curves of the fabricated electrodes at different density current from 1 to 20 A g^{-1} had been measured, which exhibit the typical galvanostatic charge-discharge curves as shown in Figure 6. All of the discharge curves for the fabricated electrodes illustrate two stages, incorporating quick potential drop firstly and then gradual potential decay to 0 V. The represented behaviors of discharge curves clearly illustrate that the capacitor mechanism for these fabricated electrodes should be the co-existence of the electric double-layer capacitance originated from the charge separation between the interface of electrode and electrolyte and the pseudo-capacitive characteristic of the electrode. In consistent with the results of CV curves, the electrode composed of Ni/P/N/C-500 exhibits the longest discharging time, compared to not only the series of hierarchical derivatives in this work, but also the other MOFs-based derivatives (Table S5).

The excellent capacitance performance of electrode composed of Ni/P/N/C-500 has been further validated by the detailed values of the specific capacitance C (farads per gram), which had been calculated according to the equation of C = $It/m\Delta V$ based on the discharge curves, as shown in Figure 6f. Herein, the parameters of I, s, m and ΔV mean the applied constant current during the process of charge-discharge, consumed time used in the process of discharge, mass (g) of the active sample in the fabricated electrode and the potential range with the unit of A, s, g and V, respectively. Observed from the calculated values, Ni/P/N/C-500 electrode exhibits the most efficient performance compared to other electrodes, as listed in Table S5. At a current density of 1 A g^{-1}, the specific capacitance of Ni/P/N/C-500 electrode is calculated as 2887.87 F g^{-1}, and along with the increase of current densities up to 20 A g^{-1}, the value decreases to 1496.96 F g^{-1}. The decreasing tendency is normally observed due to the poor availability of electrode-active sites at high at high current densities.[22-26] With the consideration of the excellent performance of Ni/P/N/C-500 electrode, the unique structure and uniformly distributed components must be responsible for such good electrochemical behavior.
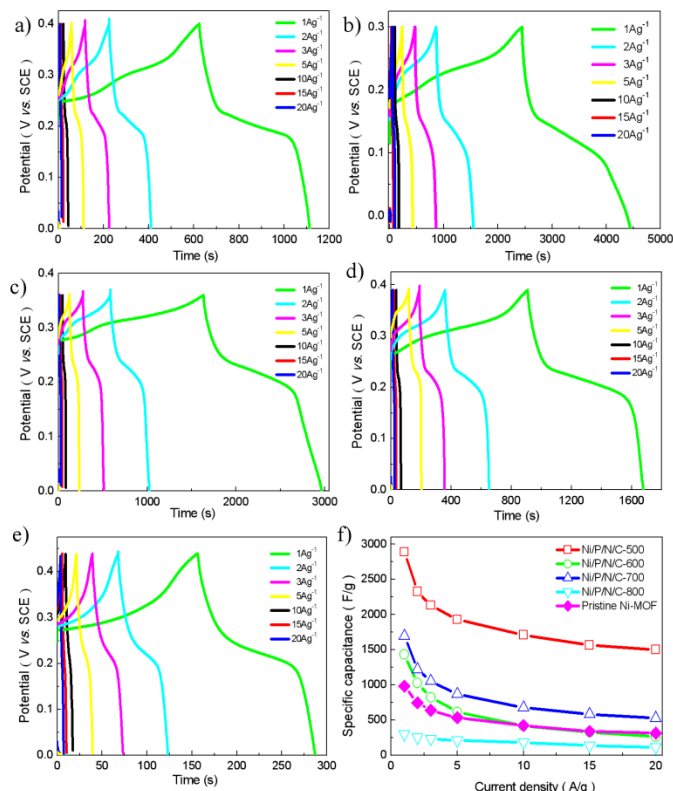
Figure 6. The galvanostatic charge-discharge curves of pristine MOF (a), Ni/P/N/C-500 (b), Ni/P/N/C-600 (c), Ni/P/N/C-700 (d) and Ni/P/N/C-800 (e) at the current density of 1-20 A g-1 in 6 M potassium hydroxide aqueous solution; (f) The comparison of specific capacitance of five fabricated electrodes at different current densities.

The excellent electrochemical performance of Ni/P/N/C-500 electrode could be further validated by the interpenetration of electrical conductivity and ion diffusion. The plots of Nyquist impedance had been measured, which are shown in Figure 7. In the low frequency regions, all the curves show the almost straight lines, which are ascribed to the pseudo-capacitive characteristic of the fabricated electrodes. In the high frequency regions, the values of equivalent series resistance (ESR) for each electrode could be conducted from the intercepts with real axis, which could illustrate the sums of intrinsic resistance of the whole electrode, electrolyte and the contact resistance between them. The corresponding values are 0.39, 0.42, 0.86, 0.47 and 0.45 Ω for pristine MOF, Ni/P/N/C-500-800. Although the similar ESR value with the pristine MOF had been presented, the smallest diameter of the semicircle in the Ni/P/N/C-500 electrode illustrates the smallest charge transfer resistance.[41-45] Comprehensively, the Ni/P/N/C-500 electrode should exhibit the lowest resistance, and is favour for electron transport in the electrode. Since the most efficient performance, the cycling performances of Ni/P/N/C-500 electrode had been further evaluated by cycling measurements. As shown in Figure S4, almost 90% effect could be retained after 1000 continuous cycling test at a current density of 10 A g^{-1}, illustrating the satisfied endurance in the practical application.

Except for the excellent performance of Ni/P/N/C-500 electrode, both Ni/P/N/C-600 and -700 electrodes also exhibit

the high-efficient performance compared to other reported electrodes (Table S5), further manifesting the important role of the title Ni-MOF as the scarified template for fabricating the excellent hierarchical derivatives used in supercapacitor electrodes. The unique structural advantages of hierarchical derivatives must be responsible for the highly efficient performance in electrochemical energy storage: 1) After thermal treatment, the proper porosity could be reserved in the final material, which ensure not only the enough surface area and channel for the transmission of ions and electrons, but also the abundant contact interfaces between the layers of electrode and electrolyte;[41,50] 2) The resulted derivatives possess multi-components as Ni, P, N, O and C that distribute uniformly in the whole material, which would supply the specific synergistic effect for improving the effective utilization of the active materials; 3) the decorated hybrid atoms as oxygen, nitrogen and phosphor atoms could improve the wettability to electrolyte solution and enhance the conductivity, resulting in the satisfied electron-transfer resistance. In addition, the best performance for Ni/P/N/C-500 should be ascribed to its specific components, proper porous surface and smallest charge transfer resistance compared to other hierarchical derivatives. The porous surface is not large, which might be more suitable for the electric double layer capacitor. The existence of nickel atom in Ni/P/N/C-500 might be also responsible for enhancing the effect of pseudocapacitors and the generation of excellent synergistic effect to improve the performance in supercapacitor. For example, although the higher nickel content in Ni/P/N/C-800 could be observed, the low performance might be ascribed to the lack of the effective synergistic effect between the versatile components.
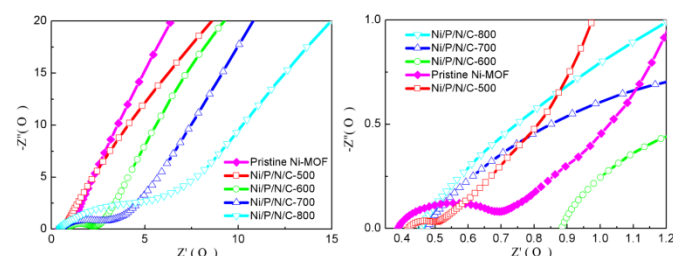
Figure 7. Nyquist plots and the enlarged plots of the five fabricated electrodes.

Conclusions

In summary, to explore the possibility of fabricating multi-components active materials used in supercapacitor, an excellent MOF template had been constructed by the careful selection of starting reactants, and then the effect of post-treatment temperature to the title MOF template had been explored. The hierarchical derivatives containing the desired Ni/P/N/C elements had been fabricated by controlling the annealing temperature, which represents the rare examples that simultaneously and uniformly incorporate these elements into one material used for supercapacitor. Through systematic electrochemical characterizations, these materials have

manifested the excellent capacitance compared to the reported active materials, especially Ni/P/N/C-500 exhibits the highest specific capacitance and the good endurance, superior to the other hierarchical composites and setting up a new benchmark in the related field. The maximum specific capacitance of Ni/P/N/C-500 electrode could be reach 2887.87 F g^{-1} at a current density of 1 A g^{-1} , along with the high capacitance of 90% retained after 1000 cycles at a current density of 10 A g^{-1} in 6M KOH solution. The high-efficient performance of these derivatives must be originated from the structural advantages inherited from the title MOF template, such as the porous structure and evenly distributed multi-components. Therefore, the related results not only reflect the important role of the selected MOF template, but also the key factor of the post-fabrication conditions for derivatives. The successful fabrication of Ni/P/N/C hybrid electrode materials via the pre-designed MOF template open up facile avenue to explore the anticipated high-efficient supercapacitor electrode, which would prompt the rapid development of related industry.

Conflicts of interest

There are no conflicts to declare.

Acknowledgements

Notes and references

1   A. J. Amali, J. Sun and Q. Xu, *Chem. Commun.*, 2014, **50**, 1519-1522.
2   A. Borenstein, O. Hanna, R. Attias, S. Luski, T. Brousse and D. Aurbach, *J. Mater. Chem. A.*, 2017, **5**, 12653-12672.
3   F. Cao, M. Zhao, Y. Yu, B. Chen, Y. Huang, J. Yang, X. Cao, Q. Lu, X. Zhang, Z. Zhang, C. Tan and H. Zhang, *J. Am. Chem.Soc.*, 2016, **138**, 6924-6927.
4   W. Chaikittisilp, M. Hu, H. Wang, H. Huang, T. Fujita, K. C. W. Wu, L. Chen, Y. Yamauchi and K. Ariga, *Chem. Commun.*, 2012, **48**, 7259-7261.
5   B. Wang, X. L. Lv, D. W. Feng, L. H. Xie, J. Zhang, M. Li, Y. B. Xie, J. R. Li and H.-C. Zhou, *J. Am. Chem. Soc.*, 2016, **138**, 6204-6216.
6   Y. L. Hu, M. L. Ding, X. Q. Liu, L. B. Sun and H. L. Jiang, *Chem. Commun.*, 2016, **52**, 5734-5737.
7   S. Gadipelli and Z. X. Guo, *Prog. Mater. Sci.*, 2015, **69**, 1-60.
8   B. Y. Guan, A. Kushima, L. Yu, S. Li, J. Li and X. W. D. Lou, *Adv. Mater.*, 2017, **29**.
9   A. Kumar, G. Hegde, S. Aruni Bt Abdul Manaf, Z. Ngaini and K. V. Sharma.*Chem. Commun.*, 2014, **50**, 12702-12705.
10 C. Guan, W. Zhao, Y. Hu, Z. Lai, X. Li, S. Sun, H. Zhang, A. K. Cheetham and J. Wang, *Nanoscale Horiz.* , 2017, **2**, 99-105.
11 H. Hu, B. Y. Guan and X. W. D. Lou, *Chem.*, 2016, **1**, 102-113.
12 G. A. M. Ali, A. Divyashree, S. Supriya, Kwok Feng Chong, A. S. Ethiraj, M. V. Reddy, H. Algarni and G. Hegde. *Dalton Trans.*, 2017, **46**, 14034-14044.
13 J. Jeon, R. Sharma, P. Meduri, B. W. Arey, H. T. Schaef, J. L. Lutkenhaus, J. P. Lemmon, P. K. Thallapally, M. I. Nandasiri, B. P. McGrail and S. K. Nune, *Acs. Appl. Mater. Inter.*, 2014, **6**, 7214-7222.
14 Y. Jiang, L. Chen, H. Zhang, Q. Zhang, W. Chen, J. Zhu and D. Song, *Chem. Eng. J.*, 2016, **292**, 1-12.
15 Y. Jiao, J. Pei, D. Chen, C. Yan, Y. Hu, Q. Zhang and G. Chen, *J. Mater. Chem. A.*, 2017, **5**, 1094-1102.
16 B. Li, M. Zheng, H. Xue and H. Pang, *Inorg. Chem. Front.*, 2016, **3**, 175-202.
17 X. Li, C. Hao, B. Tang, Y. Wang, M. Liu, Y. Wang, Y. Zhu, C. Lu and Z. Tang, *Nanoscale* , 2017, **9**, 2178-2187.
18 B. Liu, H. Shioyama, H. Jiang, X. Zhang and Q. Xu, *Carbon*, 2010, **48**, 456-463.
19 X. Liu, C. Shi, C. Zhai, M. Cheng, Q. Liu and G. Wang, *Acs. Appl. Mater. Inter.*, 2016, **8**, 4585-4591.
20 Y. Lv, L. Gan, M. Liu, W. Xiong, Z. Xu, D. Zhu and D. S. Wright, *J. Power Sources*, 2012, **209**, 152-157.
21 X. Ma, L. Zhang, G. Xu, C. Zhang, H. Song, Y. He, C. Zhang and D. Jia, *Chem. Eng. J.*, 2017, **320**, 22-28.
22 F. Meng, Z. Fang, Z. Li, W. Xu, M. Wang, Y. Liu, J. Zhang, W. Wang, D. Zhao and X. Guo, *J .Mater. Chem. A.*, 2013, **1**, 7235-7241.
23 Q. Meng, K. Cai, Y. Chen and L. Chen, *Nano Energy*, 2017, **36**, 268-285.
24 M. H. Naveen, K. Shim, M. S. A. Hossain, J. H. Kim and Y. Shim, *Adv. Energy Mater.*, 2017, **7**.
25 L. Oar-Arteta, T. Wezendonk, X. Sun, F. Kapteijn and J. Gascon, 2017, **1**, 179-1745.
26 P. Pachfule, D. Shinde, M. Majumder and Q. Xu, *Nat. Chem.*, 2016, **8**, 718-724.
27 C. Qu, L. Zhang, W. Meng, Z. Liang, B. Zhu, D. Dang, S. Dai, B. Zhao, H. Tabassum, S. Gao, H. Zhang, W. Guo, R. Zhao, X. Huang, M. Liu and R. Zou, *J .Mater. Chem. A.*, 2018, **6**, 4003-4012.
28 W. Ren, H. Zhang, C. Guan and C. Cheng, *Adv. Funct. Mater.*, 2017, **27**.
29 R. R. Salunkhe, Y. Kamachi, N. L. Torad, S. M. Hwang, Z. Sun, S. X. Dou, J. H. Kim and Y. Yamauchi, *J .Mater. Chem. A.*, 2014, **2**, 19848-19854.
30 R. R. Salunkhe, Y. V. Kaneti and Y. Yamauchi, *Acs. Nano*, 2017, **11**, 5293-5308.
31 S. Yuan, J. Qin, J. Su, B. Li, J. Li, W. Chen, H. F. Drake, P. Zhang, D. Yuan, J. Zuo and H. Zhou, *Angew. Chem. Int. Edit.*, 2018, **57**, 12578-12583.
32 X. Wang, W. Gao, Z. Niu, L. Wojtas, J. A. Perman, Y. Chen, Z. Li, B. Aguila and S. Ma, *Chem. Comm.*, 2018, **54**, 1170-1173.
33 A. J. Rieth and M. Dinca, *J. Am. Chem. Soc.*, 2018, **140**, 3461-3466.
34 C. Peng, Z. Zhuang, H. Yang, G. Zhang and H. Fei, *Chem. Sci.*, 2018, **9**, 1627-1633.
35 J. Pang, S. Yuan, J. Qin, M. Wu, C. T. Lollar, J. Li, N. Huang, B. Li, P. Zhang and H. Zhou, *J. Am. Chem. Soc.*, 2018, **140**, 12328-12332.
36 H. Molavi, M. Zamani, M. Aghajanzadeh, H. K. Manjili, H. Danafar and A. Shojaei, *Appl. Organomet. Chem.*, 2018, **32**.
37 J. Li, X. Wang, G. Zhao, C. Chen, Z. Chai, A. Alsaedi, T. Hayat and X. Wang, *Chem. Soc. Rev.*, 2018, **47**, 2322-2356.
38 P. A. Kobielska, A. J. Howarth, O. K. Farha and S. Nayak, *Coordin. Chem. Rev.*, 2018, **358**, 92-107.

ARTICLE

39 J. Jiao, C. Tan, Z. Li, Y. Liu, X. Han and Y. Cui, *J. Am. Chem. Soc.,* 2018, **140**, 2251-2259.

40 Divyashree A and G. Hegde. *RSC Adv.*, 2015, **5**, 88339-88352.

41 J. Zou, P. Liu, L. Huang, Q. Zhang, T. Lan, S. Zeng, X. Zeng, L. Yu, S. Liu, H. Wu, W. Tu and Y. Yao, *Electrochim. Acta.*, 2018, **271**, 599-607.

42 M. S. Rahmanifar, H. Hesari, A. Noori, M. Y. Masoomi, A. Morsali and M. F. Mousavi, *Electrochim. Acta.*, 2018, **275**, 76-86.

43 C. Lin and C. C. L. McCrory, *Acs. Catal.*, 2016, **7**, 443-451.

44 Y. Zhang, H. Chen, C. Guan, Y. Wu, C. Yang, Z. Shen and Q. Zou, *Acs. Appl. Mater. Inter.*, 2018, **10**, 18440-18444.

45 C. Young, J. Wang, J. Kim, Y. Sugahara, J. Henzie and Y. Yamauchi, *Chem. Mater.*, 2018, **30**, 3379-3386.

46 J. Duan, S. Chen and C. Zhao, *Nat. Commun.*, 2017, **8**, 15341.

47 J. Cong, H. Xu, M. Lu, Y. Wu, Y. Li, P. He, J. Gao, J. Yao and S. Xu, *Chem. – A. Asian J.*, 2018, **13**, 1485-1491.

48 X. Wang, L. Dong, M. Qiao, Y. Tang, J. Liu, Y. Li, S. Li, J. Su and Y. Lan, *Angew. Chem. Int. Edit.*, 2018, **57**, 9660-9664.

49 P. Du, Y. Dong, C. Liu, W. Wei, D. Liu and P. Liu, *J. Colloid Interf. Sci.,* 2018, **518**, 57-68.

50 H. Sun, Y. Lian, C. Yang, L. Xiong, P. Qi, Q. Mu, X. Zhao, J. Guo, Z. Deng and Y. Peng, *Energ. Environ. Sci.*, 2018, **11**, 2363-2371.

51 C. Shi, M. Chen, X. Han, Y. Bi, L. Huang, K. Zhou and Z. Zheng, *Inorg. Chem. Front.*, 2018, **5**, 1329-1335.

52 Q. Chen, S. Lei, P. Deng, X. Ou, L. Chen, W. Wang, Y. Xiao and B. Cheng, *J. Mater. Chem. A.*, 2017, **5**, 19323-19332.

53 H. Liu, D. Wierzbicki, R. Debek, M. Motak, T. Grzybek, P. Da Costa and M. E. Galvez, *Fuel*, 2016, **182**, 8-16.

54 S. M. Kim, P. M. Abdala, T. Margossian, D. Hosseini, L. Foppa, A. Armutlulu, W. van Beek, A. Comas-Vives, C. Coperet and C. Mueller, *J. Am. Chem. Soc.,* 2017, **139**, 1937-1949.

55 G. Garbarino, P. Riani, L. Magistri and G. Busca, *Int. J. Hydrogen Energ.*, 2014, **39**, 11557-11565.

56 R. Song, Z. Jiang, W. Bi, W. Cheng, J. Lu, B. Huang and T. Tang, *Chem.-Eur. J*, 2007, **13**, 3234-3240.

57 Z. Jiang, R. Song, W. Bi, J. Lu and T. Tang, *Carbon*, 2007, **45**, 449-458.

58 S. Dey, S. Bhattacharjee, M. G. Chaudhuri, R. S. Bose, S. Halder and C. K. Ghosh, *Rsc Adv.,* 2015, **5**, 54717-54726.

59 Y. Zhang, Y. Zhu, Y. Cao, D. Li, Z. Zhang, K. Wang, F. Ding, X. Wang, D. Meng, L. Fan and J. Wu, *Rsc Adv*, 2016, **6**, 81989-81994.

60 Z. L. Schaefer, K. M. Weeber, R. Misra, P. Schiffer and R. E. Schaak, *Chem. Mater.*, 2011, **23**, 2475-2480.

61 M. Bououdina, D. Grant and G. Walker, *Carbon*, 2005, **43**, 1286-1292.

62 L. Wu, J. Lang, S. Wang, P. Zhang and X. Yan, *Electrochim. Acta.*, 2016, **203**, 128-135.

63 J. Zhong, A. Wang, G. Li, J. Wang, Y. Ou and Y. Tong, *J. Mater. Chem.*, 2012, **22**, 5656-5665.

64 Y. Li, L. Cao, L. Qiao, M. Zhou, Y. Yang, P. Xiao and Y. Zhang, *J. Mater. Chem. A*, 2014, **2**, 6540-6548.

Hierarchical Nickel/Phosphorus/Nitrogen/Carbon Composites Templated by One Metal-Organic Framework as Highly-Efficient Supercapacitor Electrode Materials
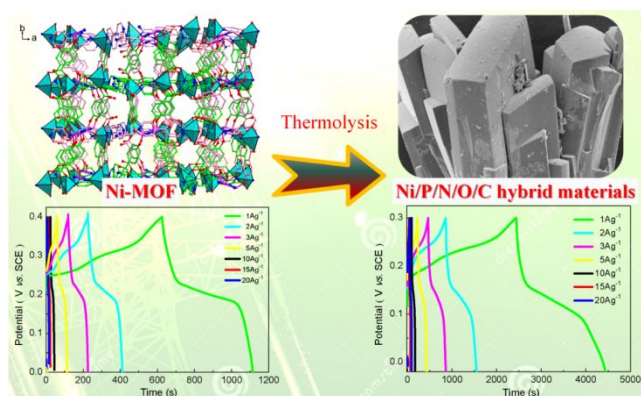
By utilization of the structural advantage of Metal-Organic Frameworks, hierarchical carbon materials containing Ni, P, N and O have been firstly fabricated, exhibiting the high performance in electrochemical energy storage.